In Silico Study of Local Electrical Impedance Measurements in the Atria - Towards Understanding and Quantifying Dependencies *in Human*

Laura Anna Unger, Carmen Martínez Antón, Michael Stritt, Reza Wakili, Annika Haas, Michael Kircher, Olaf Dössel, *Fellow, IEEE*, and Armin Luik

Abstract*—*Background: **Electrical impedance measurements have become an accepted tool for monitoring intracardiac radio frequency ablation. Recently, the long-established generator impedance was joined by novel local impedance measurement capabilities with all electrical circuit terminals being accommodated within the catheter. *Objective:* This work aims at *in silico* quantification of distinct influencing factors that have remained challenges due to the lack of ground truth knowledge and the superposition of effects in clinical settings. *Methods:* We introduced a highly detailed *in silico* model of two local impedance enabled catheters, namely IntellaNav MiFi OI and IntellaNav Stablepoint, embedded in a series of clinically relevant environments. Assigning material and frequency specific conductivities and subsequently calculating the spread of the electrical field with the finite element method yielded *in silico* local impedances. The *in silico* model was validated by comparison to *in vitro* measurements of standardized sodium chloride solutions. We then investigated the effect of the withdrawal of the catheter into the transseptal sheath, catheter-tissue interaction, insertion of the catheter into pulmonary veins, and catheter irrigation. *Results:* All simulated setups were in line with *in vitro* experiments and *in human* measurements and gave detailed insight into determinants of local impedance changes as well as the relation between values measured with two different devices. *Conclusion:* The *in silico* environment proved to be capable of resembling clinical scenarios and quantifying local impedance changes. Significance: The tool can assists the interpretation of measurements in humans and has the potential to support future catheter development.**

***Index Terms*—Ablation, atrial substrate, bioimpedance, cardiac electrophysiology, local impedance, radio frequency ablation.**

I. Introduction

ELECTRICAL impedance measurements have a long history in the medical and biomedical field. Historical studies have shown that different kinds of biological tissues are characterized by different conductivity spectra [1] attributed to the microscopic composition of the materials [2]. Besides the composition of the material and the measurement frequency, electrode arrangement and temperature are major determinants of the measured impedance.

During invasive cardiac electrophysiological studies, generator impedance measurements have been an established method to monitor the delivery of radio frequency energy during ablation since decades [3], [4]. The transthoracic impedance of the radio frequency energy delivery pathway between an intracardiac and a cutaneous dispersive electrode assists differentiation of tissue contact during ablation. However, the bulk impedance of the torso blurs measurements [5], [6] and impedes detailed assessment of tissue characteristics in the region of interest next to the catheter. Recently, two novel catheters have been introduced to the market that aim at a more locally focused impedance assessment in the vicinity of the catheter with all injecting and measuring electrodes being built into the intracardiac catheter itself [4]. The radio frequency ablation catheters IntellaNav MiFi OI [7] and IntellaNav Stablepoint [8] (Boston Scientific, Malborough, MA, USA) come with a four-electrode and a three-electrode impedance measurement circuit implemented within the catheter, respectively. During ablation, the so-called DirectSense technology measures the magnitude of the local impedance (LI). An LI drop resulting from a combination of resistive tissue heating and subsequent myocardial destruction and lesion formation is used as a surrogate for lesion quality and durability [7], [9]. Compared to the transthoracic generator

Manuscript received 24 January 2022; revised 14 May 2022 and 21 July 2022; accepted 23 July 2022. Date of publication 4 August 2022; date of current version 20 January 2023. This work was supported in part by the Deutsche Forschungsgemeinschaft (DFG, German Research Foundation) – Project-ID 394433254 (LU 2294/1-1, DO 637/23-1) and in part by the European Union's Horizon 2020 Research and Innovation Programme under the Marie-Sklodowska-Curie under Grant 860974. *(Corresponding author: Laura Anna Unger.)*

Laura Anna Unger is with the Institute of Biomedical Engineering, Karlsruhe Institute of Technology, 76131 Karlsruhe, Germany (e-mail: publications@ibt.kit.edu).

Carmen Martínez Antón, Michael Stritt, and Olaf Dössel are with the Institute of Biomedical Engineering, Karlsruhe Institute of Technology, Germany.

Reza Wakili is with the West German Heart and Vascular Center, University Hospital Essen, Germany.

Annika Haas and Armin Luik are with the Medizinische Klinik IV at Städtisches Klinikum Karlsruhe, Academic Teaching Hospital of the University of Freiburg, Germany.

Michael Kircher was with the Institute of Biomedical Engineering, Karlsruhe Institute of Technology, Germany. He is now with the Carl Zeiss Meditec AG, Germany.

Digital Object Identifier 10.1109/TBME.2022.3196545

impedance, the LI emphasizes local changes in impedance while being less susceptible to far field artifacts [9]–[12]. Despite an increased influence of the local surroundings on the measurement compared to the generator impedance, the LI is still sensitive to the three-dimensional arrangement of materials and their properties surrounding the catheter [13]. LI may therefore not be mistaken for lumped impedance measurements, which condense all influencing properties to an infinitesimal element. Besides the monitoring of ablation lesion formation, LI has also shown potential to characterize cardiac tissue and differentiate between healthy myocardium and fibrotic or scar tissue [10]–[12]. Atrial fibrillation as the most common sustained cardiac arrhythmia poses a major burden for both patients and global health care systems. Since current treatment approaches result in unsatisfactory success rates, novel methods of tissue characterization such as the LI need further exploration.

A major challenge in the expansion of the diagnostic value of intracardiac LI measurements are confounding factors. Not only different tissue compositions but also the distance and angle between the catheter and the tissue, the surrounding tissue geometry, an overlap of catheter and transseptal sheath, and sodium chloride (NaCl) solution irrigation influence the measurement, amongst others. Many of these effects can be observed in *in human* studies but lack quantification due to the superposition of multiple effects and an unknown ground truth. Therefore, the differentiation between the target measure and confounding factors has remained uncertain. *In vitro* and *ex vivo* experiments can help to shed light on different scenarios but are costly and depending on the experimental setup, the underlying ground truth still remains under-determined.

In this work, we present for the first time a highly detailed *in silico* framework that models the IntellaNav MiFi OI catheter and the IntellaNav Stablepoint catheter in combination with different clinically relevant surroundings. After validation of the framework by *in vitro* measurements in standardized setups, clinically relevant scenarios such as the effect of the distance and angle between catheter and tissue, scar tissue, the insertion of the catheter into a pulmonary vein or a transseptal sheath, and NaCl solution irrigation were investigated and compared to *in vitro* and *in human* measurements.

With a highly detailed comparison between different catheter geometries and the investigation of isolated scenarios to quantify various clinically relevant effects, this work paves the way for an inexpensive enhancement of the understanding of intracardiac LI measurements and future catheter development.

II. Methods

A. In Silico — Geometrical Setup

Both clinically available LI enabled radio frequency ablation catheters were modeled in high detail as depicted in Fig. 1(a) to (d). Measures were taken from product specification sheets [14], [15] as well as calibrated photographs yielding a resolution below 100 μm.

The IntellaNav MiFi OI comes with a 4.5 mm tip electrode, three ring electrodes of 1.3 mm width and 2.5 mm spacing,

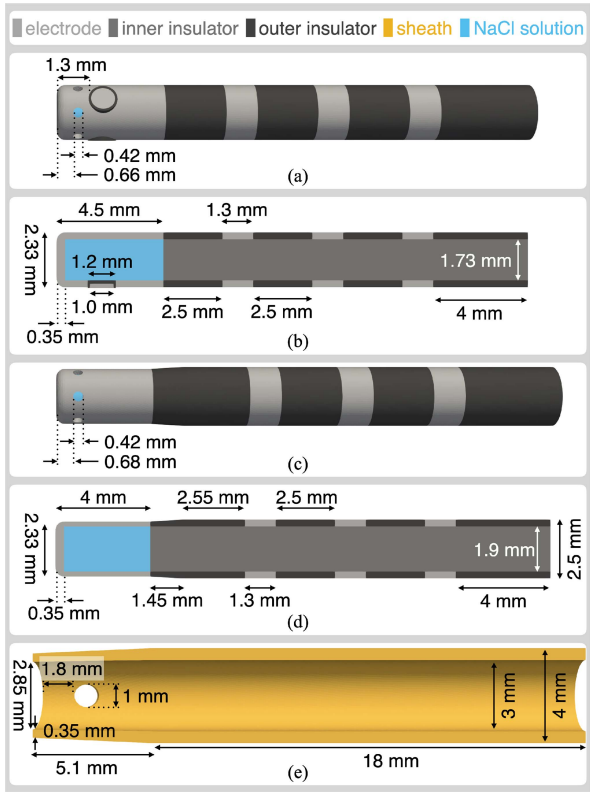

Fig. 1. Geometrical models of LI enabled radio frequency ablation catheters and a transseptal sheath. (a) 3D model of the IntellaNav MiFi OI. (b) Cross-section of the IntellaNav MiFi OI. (c) 3D model of the IntellaNav Stablepoint. (d) Cross-section of the IntellaNav Stablepoint. (e) Cross-section of a transseptal sheath including one out of two irrigation holes.

three evenly distributed mini electrodes of 0.8 mm diameter embedded in the tip electrode, six irrigation holes, and a cooling chamber filled with NaCl solution. The interior of the catheter is electrically isolated from the electrodes and accommodates thin electrical and mechanical steering wires. While neglecting the latter, the interior of the catheter shaft was filled with insulating material in the model.

The IntellaNav Stablepoint is similarly composed of a 4 mm tip electrode, three ring electrodes of 1.3 mm width and 4.0 mm | 2.5 mm | 2.5 mm spacing, six irrigation holes, and a cooling chamber filled with NaCl solution. The tip does not embed any mini electrodes. Proximal to the tip, the diameter expands conically to the shaft diameter. The existence of the force sensing spring between the tip electrode and the distal ring electrode in the interior of the catheter [8] was assumed to be negligible with respect to the spread of the electrical field outside the catheter. Therefore, the interior of the catheter shaft was filled with insulating material as well.

A transseptal sheath was implemented on the model of the 8.5 F Agilis NxT steerable introducer (Abbott, Chicago, IL, USA) as depicted in Fig. 1(e).

Detailed measures of the implemented catheter and sheath geometries are shown in Fig. 1.

The respective catheter was embedded in a 140 mm $\times$ 140 mm $\times$ 140 mm box filled with either blood or NaCl solution

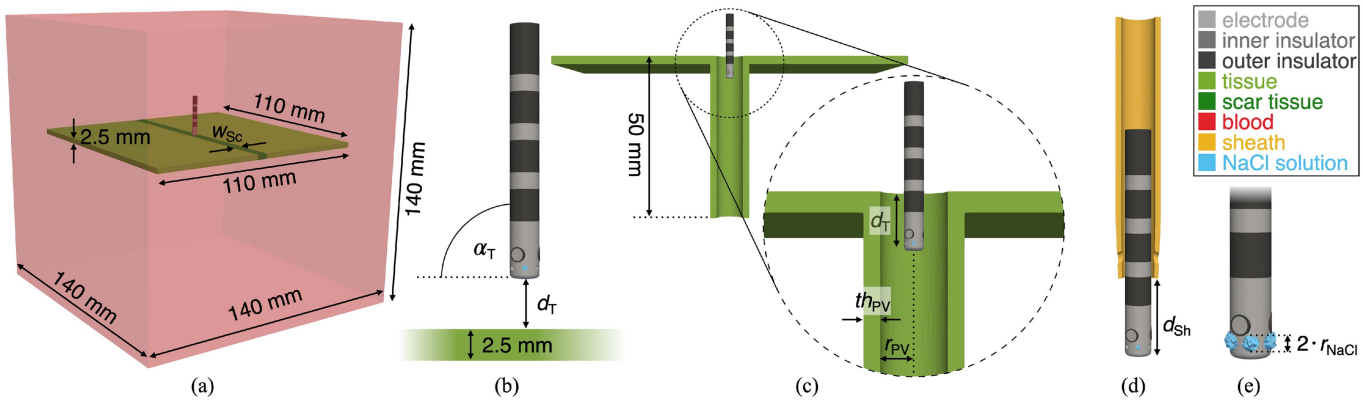

Fig. 2. Simulation setups. All setups are depicted at the example of the IntellaNav MiFi OI and were equally conducted with the IntellaNav Stablepoint. (a) Tissue patch with line of scar within the surrounding blood box. (b) Variation of distance and angle between catheter and tissue. (c) Insertion of the catheter into the PV. (d) Insertion of the catheter into the transseptal sheath. (e) Irrigation with NaCl solution.

as displayed in Fig. 2(a) for all simulation setups. Geometry definition and tetrahedral meshing was done with Gmsh (version 4.5.6) [16]. Mesh resolution was adapted to the size of local structures being the highest at the IntellaNav MiFi OI mini electrodes and the lowest at the outer boundary of the surrounding box. The meshes were comprised of 2.5 million to 5 million tetrahedral elements.

1) Standardized NaCl Solutions: Either catheter was placed in the surrounding box filled with NaCl solution of eight different molar concentrations starting from 0.02 $\frac{\text{mol}}{\text{l}}$ in steps of 0.01 $\frac{\text{mol}}{\text{l}}$ up to 0.09 $\frac{\text{mol}}{\text{l}}$.

2) Transseptal Steerable Sheath: Within a surrounding box filled with blood, either catheter was withdrawn into the transseptal sheath model with the distance d_{Sh} describing the distance between the catheter tip and the distal edge of the sheath (compare Fig. 2(d)). Negative distances describe the withdrawal of the catheter into the sheath. d_{Sh} was varied from -2 mm in steps of 0.5 mm up to 19.5 mm.

3) Tissue: Either catheter was placed in the surrounding box filled with blood. A square patch of tissue measuring 110 mm $\times$ 110 mm $\times$ 2.5 mm was placed below the catheter resembling a piece of atrial myocardial tissue of typical wall thickness [17] (compare Fig. 2(a)). The distance d_{T} between the catheter and the tissue was varied from -2 mm to 10 mm in steps of 0.5 mm (compare Fig. 2(b)). Negative distances represented an immersion of the catheter into the tissue. Mechanical interaction was not modeled. Instead, the catheter simply displaced the tissue.

In a second step, the angle α_{T} between the catheter and the tissue was varied from 0° to 180° in steps of 15°. For $90° < \alpha_{\text{T}} \leq 180°$, one of the mini electrodes pointed directly towards the tissue. For $0° \leq \alpha_{\text{T}} < 90°$, the two remaining electrodes were pointed towards — but not directly towards — the tissue (compare Fig. 2(b)). The pivot was located at the intersection of the catheter's distal plane and the outer wall of the catheter shaft at the left and the right, respectively. The experiment was conducted for five different distances between catheter and tissue $d_{\text{T}} \in \{0.0\,\text{mm}, 0.5\,\text{mm}, 1.0\,\text{mm}, 2.0\,\text{mm}, 4.0\,\text{mm}\}$.

4) Transmural Lesion: The general tissue setup as described above was complemented by a central line of scar tissue of width $w_{\text{Sc}} \in \{3\,\text{mm}, 6\,\text{mm}\}$ (compare Fig. 2(a)) representing ablated tissue from a previous procedure or natively developed myocardial scar. For two different distances between catheter and tissue ($d_{\text{T}} = 0\,\text{mm}$ and $d_{\text{T}} = 1\,\text{mm}$), either catheter was moved perpendicularly to the line of scar starting at a distance to the center of the line of scar of $d_{\text{Sc}} = -10\,\text{mm}$, crossing the line of scar for $d_{\text{Sc}} = 0\,\text{mm}$ up to a distance of $d_{\text{Sc}} = 10\,\text{mm}$ at a default step size of 1 mm and a decreased step size of 0.5 mm for $|d_{\text{Sc}}| < 2\,\text{mm}$.

5) Pulmonary Vein: The insertion of either catheter into a pulmonary vein (PV) was simulated by extending the general tissue setup by a perpendicular tube filled with blood (compare Fig. 2(c)). For a PV wall thickness $th_{\text{PV}} = 2\,\text{mm}$, four different inner PV radii $r_{\text{PV}} \in \{2\,\text{mm}, 3\,\text{mm}, 4\,\text{mm}, 6\,\text{mm}\}$ were implemented. For $r_{\text{PV}} = 6\,\text{mm}$, additional PV wall thicknesses of $th_{\text{PV}} \in \{1\,\text{mm}, 3\,\text{mm}, 4\,\text{mm}\}$ were modeled. Either catheter was inserted into the PV quantified by the distance d_{T} to the surface of the tissue. Negative distances represent states with the respective catheter being inside the PV while positive distances represent states of catheter elevation above the tissue. d_{T} was varied from -20 mm (full immersion) to 10 mm (full extraction) in steps of 1 mm.

6) Irrigation: Catheter irrigation was modeled by placing a sphere of physiological NaCl solution at each center of the irrigation holes displacing all encircled blood elements (compare Fig. 2(e)). The radius r_{NaCl} of the NaCl spheres was varied from 0 mm to 2 mm in steps of 0.05 mm.

B. In Silico — Material Properties

The tetrahedral elements of the geometrical meshes were assigned conductivity values characteristic for the respective material at 14.5 kHz as summarized in Table I. Due to the significant dependency of conductivities on the temperature, the latter had to be regarded for.

The *in vitro* setups with NaCl solutions of different concentrations were conducted at different temperatures and compared to *in silico* experiments based on conductivities published by Gabriel et al. [1], which lack an explicit statement about temperature. Comparing to the conductivity of 0.5 % NaCl solution given for 20 °C [18] suggests that Gabriel et al. measured at

TABLE I
CONDUCTIVITIES OF RELEVANT MATERIALS AT 14.5 KHZ

Material	Conductivity σ (S/m)	Temperature (°C)	Reference
metallic electrode	$400,000$		[20]
insulator	10^{-7}		
sheath	10^{-7}		
blood	0.700	BT	[21] [22]
myocardial tissue	0.164	BT	[21] [22]
connective tissue (scar)	0.387	BT	[21] [22]
NaCl 0.020 $\frac{\text{mol}}{\text{l}}$ (0.12 %)	0.220	T_{Gab}	[1]
NaCl 0.030 $\frac{\text{mol}}{\text{l}}$ (0.18 %)	0.330	T_{Gab}	[1]
NaCl 0.040 $\frac{\text{mol}}{\text{l}}$ (0.23 %)	0.430	T_{Gab}	[1]
NaCl 0.050 $\frac{\text{mol}}{\text{l}}$ (0.29 %)	0.530	T_{Gab}	[1]
NaCl 0.060 $\frac{\text{mol}}{\text{l}}$ (0.35 %)	0.620	T_{Gab}	[1]
NaCl 0.070 $\frac{\text{mol}}{\text{l}}$ (0.41 %)	0.720	T_{Gab}	[1]
NaCl 0.080 $\frac{\text{mol}}{\text{l}}$ (0.47 %)	0.800	T_{Gab}	[1]
NaCl 0.086 $\frac{\text{mol}}{\text{l}}$ (0.50 %)	0.820	20	[18]
NaCl 0.090 $\frac{\text{mol}}{\text{l}}$ (0.53 %)	0.880	T_{Gab}	[1]
NaCl 0.154 $\frac{\text{mol}}{\text{l}}$ (0.90 %)	1.444	20	
NaCl 0.171 $\frac{\text{mol}}{\text{l}}$ (1.00 %)	1.600	20	[18]

BT: Body Temperature; T_{Gab}: Measurement Temperature in Gabriel et al. [1]

a slightly higher temperature T_{Gab} (compare Table I). With a temperature coefficient of approximately $2.1\frac{\%}{^\circ}$ [19] and the reference values from [18], Gabriel et al. most likely measured NaCl solutions significantly below body temperature as opposed to their measurements of biological tissue. Since the data set [1] was consistent in itself, the exact temperature was deemed insignificant for the validation setups with NaCl solutions of different concentrations.

All other *in silico* experiments were parameterized with conductivities given for blood, myocardial tissue, and scar tissue at body temperature (BT) as well as physiological 0.9 % NaCl solution for catheter irrigation at an approximate lab temperature of 20 °C as listed in Table I. Due to the lack of an explicit reference for the conductivity of physiological 0.9 % NaCl solution, the latter was linearly interpolated from the conductivities of 0.5 % and 1 % NaCl solution at 20 °C [18] as listed in Table I.

C. In Silico — Impedance Forward Simulation

The spread of the electrical field was simulated with the software EIDORS v3.10 [23] and MATLAB R2021a (The MathWorks, Inc., Natick, MA, USA). In short, EIDORS solves the Poisson equation with a finite element model F. The injection currents are given as boundary conditions. The current density and the potential field are the solution. The voltage v between two electrodes is extracted as the potential difference and is dependent on the given conductivities $\boldsymbol{\sigma}$ at the elements of the model and the stimulation pattern $\boldsymbol{q}$ of the electrode model with $v = F(\boldsymbol{\sigma}, \boldsymbol{q})$ [23].

Stimulation and measurement circuits were defined according to the clinical system: A four-terminal circuit with current injection between the distal tip electrode and the proximal ring electrode was combined with measurements between the mini electrodes and the distal ring electrode for the IntellaNav MiFi OI [7]. The three voltage measurements resulting from either mini electrode to the distal ring electrode were reduced to their maximum value following the clinical system. The IntellaNav Stablepoint was set up as a three-terminal circuit with current injection between the distal tip electrode and the proximal ring electrode and voltage measurement between the distal tip electrode and the distal ring electrode.

An alternating current of $5\,\mu$A peak-to-peak amplitude at 14.5 kHz was modeled. The complete electrode model was used [24]. The resulting voltage amplitude $|v|$ was then divided by the amplitude of the injected current to obtain LI as the magnitude of the impedance.

D. In Vitro Setup

All measurements were conducted with the Rhythmia HDx system (Boston Scientific, Malborough, MA, USA), the IntellaNav MiFi OI, and the IntellaNav Stablepoint. To validate the simulation framework, NaCl solutions of different concentrations and known conductivity σ were prepared. The molar mass as given in [1] starting from 0.02 $\frac{\text{mol}}{\text{l}}$ up to 0.09 $\frac{\text{mol}}{\text{l}}$ in steps of 0.01 $\frac{\text{mol}}{\text{l}}$ was converted to weight percentages. The respective amount of NaCl was weighed out with a scale of 10^{-3} g resolution and 10^{-3} g precision and dissolved in 250 ml of de-ionized water. For all concentrations, the NaCl dissolved completely and formed an aqueous solution. A thermometer of 0.1 °C resolution was used to keep track of the solution's temperature. The LI was measured with both catheters in each solution at 7 to 13 different temperatures between 18.2 °C and 38.8 °C. For comparability, the LI at three different temperatures — namely 21 °C, 25 °C, and 36 °C — was interpolated and compared to the simulated results for the respective NaCl solutions.

Additionally, the behavior of LI with tissue contact was measured *in vitro*. A tissue phantom composed of 100 ml de-ionized water, 3 g agar-agar, and 0.0499 g NaCl [25] was prepared. The expected conductivity of 0.16 $\frac{\text{S}}{\text{m}}$ at 25 °C matched the conductivity of cardiac tissue at 14.5 kHz well. Since *in vitro* measurements were taken at 20.5 °C in this work, the actual conductivity might have deviated slightly due to the difference in temperature. Typical temperature coefficients reported for similar materials justified to neglect deviations caused by the described change in temperature [19], [26]. Additionally, a piece of smooth left atrial porcine tissue was used. The tissue phantom and the tissue sample were mounted at an elevated ring in order not to disturb measurements by the mount in 0.35 % NaCl solution. Either catheter was positioned at the tissue phantom and the tissue sample in orthogonal and parallel orientation.

The effect of catheter irrigation with physiological NaCl solution on LI was investigated by increasing the flow rate of the HAT 500 irrigation pump (Osypka AG, Rheinfelden, Germany) from 0 $\frac{\text{ml}}{\text{min}}$ to 2 $\frac{\text{ml}}{\text{min}}$ and 17 $\frac{\text{ml}}{\text{min}}$ in a 250 ml bath of 0.35 % NaCl solution. A flow rate of 2 $\frac{\text{ml}}{\text{min}}$ is clinically applied in standby mode while the flow rate is typically adjusted to 17 $\frac{\text{ml}}{\text{min}}$ during ablation. The bath model did not include circulation.

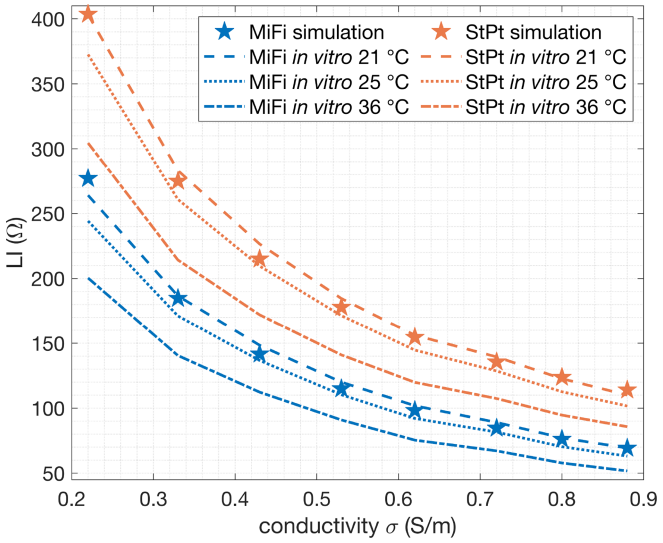

Fig. 3. *In vitro* LI measurements of several NaCl molar solutions compared with simulated LI values. Broken lines correspond to measurements at 21 °C, 25 °C, and 36 °C, whereas star marks refer to simulations. IntellaNav MiFi OI and IntellaNav Stablepoint values are shown in blue, and orange, respectively.

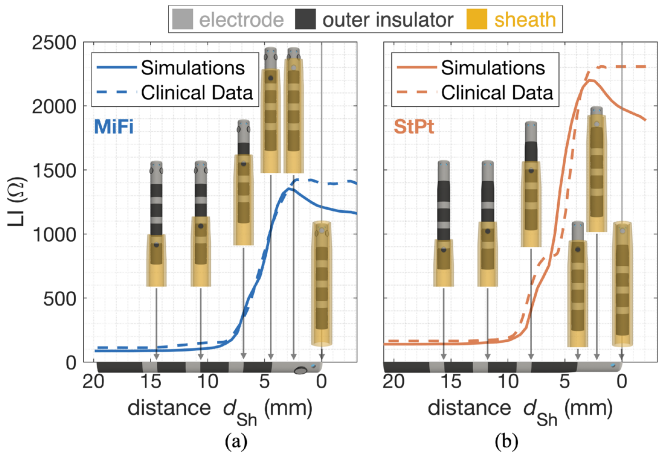

Fig. 4. Withdrawal of (a) IntellaNav MiFi OI and (b) IntellaNav Stablepoint into a transseptal sheath. *In silico* LI is represented by solid lines while clinical LI is represented by dashed lines. Sheath positions are indicated on the horizontal axes.

E. In Human Setup

Clinical measurements complemented the *in silico* analysis of catheter sheath interaction and its effect on the LI. Either catheter was located in the left atrium passing the inter-atrial septum via the transseptal sheath, namely the Agilis NxT steerable introducer. An X-ray scan verified that the proximal ring electrode was outside of the sheath. Starting from a central position in the left atrial bloodpool without endocardial contact, the catheter was gradually pulled back into the sheath at constant speed while recording the LI. Clinical LI was represented by its moving average calculated with a sliding window of 1.5 s width as provided by the electroanatomical mapping system. All *in human* measurements were approved by the local ethics committee and were conducted in accordance with the Declaration of Helsinki. Written informed consent was obtained from all patients.

III. Results

A. Aqueous NaCl Solutions

Fig. 3 presents LI values measured *in vitro* in aqueous NaCl solutions prepared according to Table I at 21 °C, 25 °C, and 36 °C along with simulated LI values for *in silico* setups of the corresponding molar concentrations. Higher temperatures yielded lower LI values for constant NaCl concentration. *In vitro* and *in silico* experiments followed the same hyperbolic-like trend with decreasing LI values for increasing conductivity.

Simulated LI values predominantly fell between the corresponding *in vitro* measurements at 21 °C and 25 °C for both catheters with a median deviation of −2.7 Ω and −2.8 Ω from the measurements at 21 °C for the IntellaNav MiFi OI and the IntellaNav Stablepoint, respectively. A negative deviation is in line with the assumption of 20 °C $< T_{\mathrm{Gab}} \ll$ 36 °C as stated in Section II-D. With the *in silico* and *in vitro* traces matching both in morphology and absolute values, the simulation environment was considered valid to a high degree of detail across the relevant range of conductivities for further experiments.

NaCl concentrations of $c_{\mathrm{NaCl}} = 0.06\ \frac{\mathrm{mol}}{\mathrm{l}}$ and $c_{\mathrm{NaCl}} = 0.07\ \frac{\mathrm{mol}}{\mathrm{l}}$ equaling mass concentrations of 0.35 % and 0.41 % were found to yield an LI comparable to human blood. For a concentration of $c_{\mathrm{NaCl}} = 0.06\ \frac{\mathrm{mol}}{\mathrm{l}}$, the *in silico* setups yielded an LI of 98.3 Ω and 154.5 Ω compared to *in vitro* measurements at 21 °C of 101.9 Ω and 156.2 Ω for the IntellaNav MiFi OI and IntellaNav Stablepoint, respectively, which compared well to the clinically observed ranges of bloodpool LI.

The simulated bloodpool LI for a blood conductivity $\sigma = 0.7\ \frac{\mathrm{S}}{\mathrm{m}}$ [22] as given in Table I and later on used in all other *in silico* setups was at the lower bound of clinically observed values with 87.1 Ω for the IntellaNav MiFi OI and 138.9 Ω for the IntellaNav Stablepoint.

Linear regression of LI measurements with both catheters deduced a perfect linear relationship ($R^2 < 10^{-4}$) between LI values measured with the IntellaNav MiFi OI (LI_{MiFi}) and the IntellaNav Stablepoint (LI_{StPt}) for *in silico* and *in vitro* experiments. Measurements in an extended set of 25 NaCl solutions of concentrations between 0.15 % and 2.00 % yielded the following linear relationship:

$$LI_{\mathrm{StPt}} = 1.42 \cdot LI_{\mathrm{MiFi}} + 8.7\,\Omega \tag{1}$$

B. Transseptal Steerable Sheath

Fig. 4 presents simulated and exemplary clinical LI traces characteristic for the withdrawal of the IntellaNav MiFi OI (a) and the IntellaNav Stablepoint (b) into the transseptal sheath.

Starting at a simulated bloodpool of 87 Ω and 139 Ω, the *in silico* LI measured with the IntellaNav MiFi OI and the IntellaNav Stablepoint first increased by more than 2 Ω for the distal edge of the sheath being located between the proximal and the 2nd to proximal ring electrode. The steep

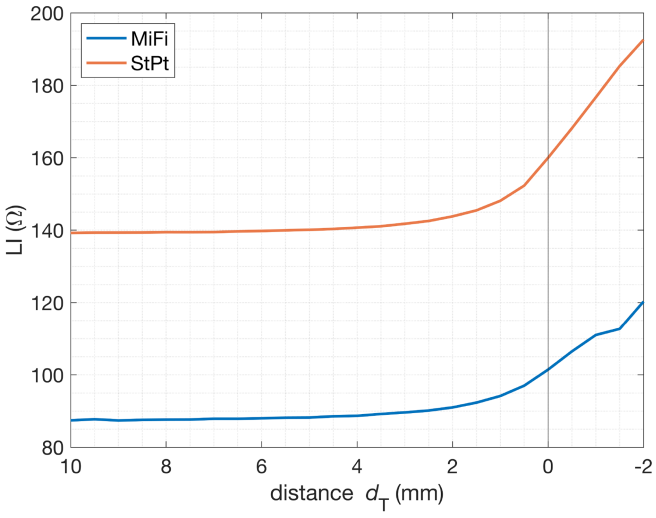

Fig. 5. Dependency of LI on the distance to myocardial tissue for IntellaNav MiFi OI in blue and IntellaNav Stablepoint in orange.

increase of LI began upon the coverage of the distal ring electrode by the sheath. For full sheath coverage, the LI increased up to 1353 Ω and 2200 Ω for the IntellaNav MiFi OI and the IntellaNav Stablepoint, respectively. For the distal edge of the sheath being located between the distal ring electrode and the tip electrode, an interim decrease in steepness formed a plateau especially pronounced for the IntellaNav Stablepoint.

Both simulated traces compared well with the clinically measured traces.

C. Catheter Tissue Interaction

1) Catheter Distance and Orientation: Again starting from a bloodpool LI of 87 Ω and 139 Ω for the IntellaNav MiFi OI and the IntellaNav Stablepoint, respectively, the LI increased with decreasing distance to the tissue surface for perpendicular catheter positions ($\alpha_T = 90°$) as shown in Fig. 5. At a distance $d_T = 3.5$ mm and $d_T = 2.5$ mm, the LI exceeded the bloodpool LI by more than 2 % for the IntellaNav MiFi OI and IntellaNav Stablepoint, respectively. At a distance $d_T = 0$ mm, the LI exceeded the bloodpool LI by 16.0 % and 14.9 % for the IntellaNav MiFi OI and IntellaNav Stablepoint, respectively. The closer the catheter approached the tissue, the steeper the LI increased. For negative distances d_T, i.e. the catheter entering the tissue, the increase in LI per distance was approximately constant. For the IntellaNav MiFi OI, a small plateau in LI formed between $d_T = -1.0$ mm and $d_T = -1.5$ mm.

Fig. 6 presents the simulated LI values for changing angles α_T between the catheter and the tissue for selected distances. For both catheters and all distances, the traces were w-shaped. Starting from a perpendicular position and approaching a parallel position, LI first dropped and then increased again. The LI for parallel catheter orientation at a distance $d_T = 0$ mm exceeded the LI for perpendicular catheter positions by 14.0 Ω ($\alpha_T = 0°$) and 12.9 Ω ($\alpha_T = 180°$) for the IntellaNav MiFi OI and by 9.4 Ω

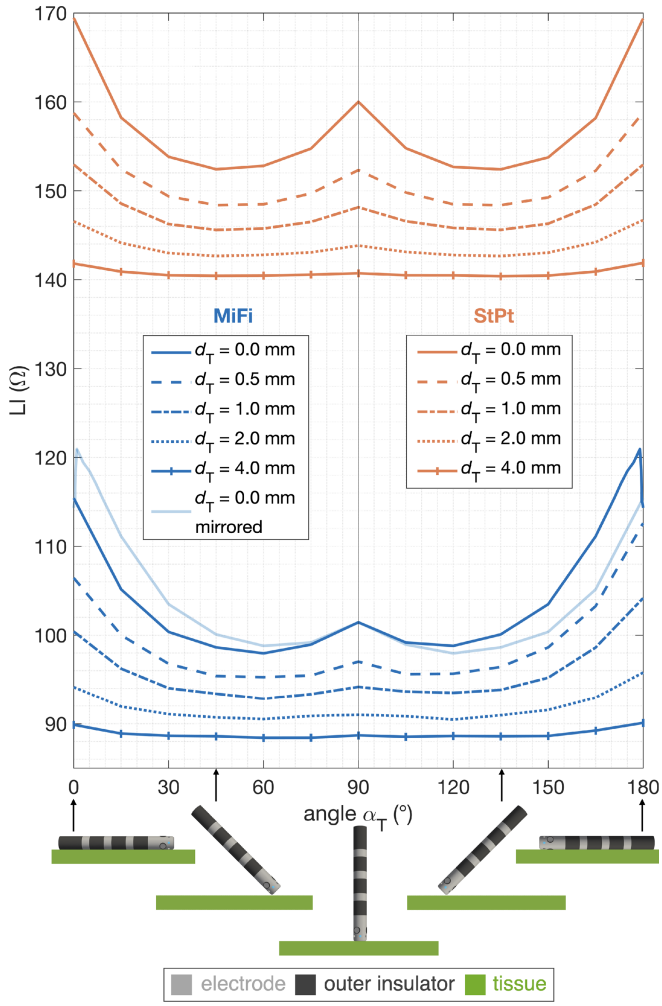

Fig. 6. Dependency of LI on the angle α_T between catheter and myocardial tissue for IntellaNav MiFi OI in blue and IntellaNav Stablepoint in orange for different distances d_T between catheter and tissue.

for the IntellaNav Stablepoint. While the traces were symmetric to $\alpha_T = 90°$ for the IntellaNav Stablepoint, the LI depended on the orientation of the mini electrodes for the IntellaNav MiFi OI as indicated by the mirrored trace in Fig. 6. Catheter orientations with one of the measuring mini electrodes being directed to the tissue ($(90° < \alpha_T \leq 180°)$) exceeded those LI values of the same distance and angle for which none of the mini electrodes pointed directly towards the tissue ($0° \leq \alpha_T < 90°$).

In vitro measurements with the respective catheter touching a tissue phantom or a tissue sample perpendicularly and in parallel yielded comparable differences between the parallel and orthogonal position. The LI for the parallel position exceeded the LI of the perpendicular position by approximately 11 Ω and 10 Ω for the IntellaNav MiFi OI and IntellaNav Stablepoint, respectively.

2) Transmural Lesion: Due to the higher conductivity of connective tissue compared to healthy myocardium, the LI typically drops in the vicinity of myocardial lesions. In these setups, the dependency of the LI on the extent of the scar and the relative position of the catheter was investigated. Fig. 7 shows LI

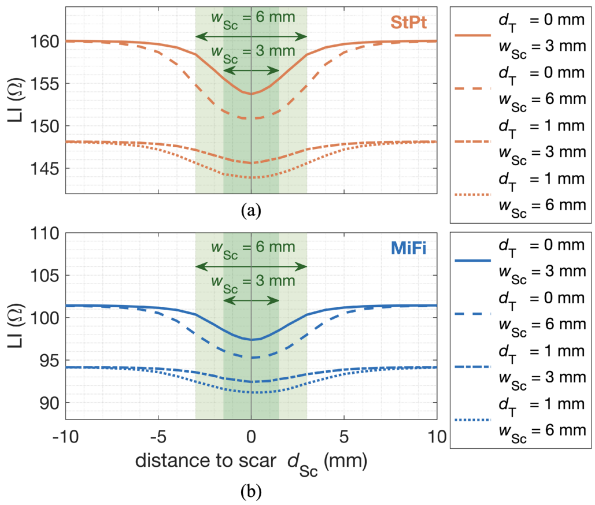

Fig. 7. Dependency of the LI on the horizontal distance d_{Sc} to a linear scar embedded in a patch of tissue for the IntellaNav MiFi OI in (a) and the IntellaNav Stablepoint in (b). Each catheter hovered the tissue at two vertical distances $d_T = 0$ mm and $d_T = 1$ mm for two different scar widths $w_{Sc} = 3$ mm and $w_{Sc} = 6$ mm.

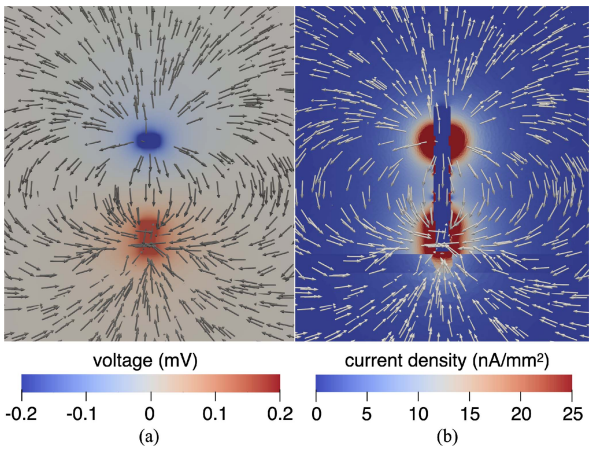

Fig. 8. Cross section of a setup with a scar of 3 mm width embedded in a patch of myocardial tissue surrounded by blood. The (a) potential field and (b) current density characterize the electrical field. Arrows mark the direction of current flow.

traces for the virtual catheter passing linear lesions of 3 mm and 6 mm width. For direct tissue contact ($d_T = 0$ mm), the absolute drop was larger for the IntellaNav Stablepoint due to the higher baseline LI for either lesion width. The percentage drop based on the LI at maximum distance to the lesion, however, was similar with 3.8 % and 6.0 % for lesion widths of 3 mm and 6 mm for the IntellaNav MiFi OI and a percentage drop of 3.9 % and 5.7 % for the IntellaNav Stablepoint. Increasing the vertical distance d_T between the catheter and the myocardial tissue by 1 mm caused a larger drop in the baseline LI than either of the scars for both catheters.

Fig. 8 shows the potential field (a) and the current density (b) for the setup with a scar width $w_{Sc} = 3$ mm and direct tissue contact. With a similarity to an electrical dipole field, the current spreads between the injecting electrodes. The current density in

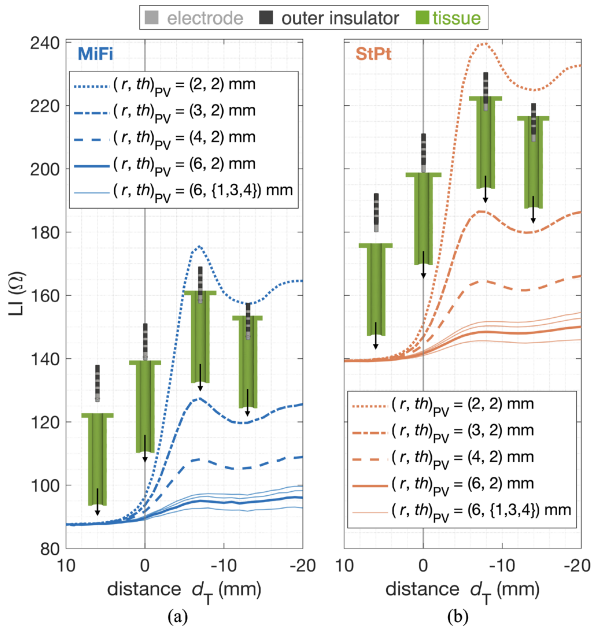

Fig. 9. LI traces upon progressive introduction of (a) IntellaNav MiFi OI in blue and (b) IntellaNav Stablepoint in orange into a PV. The horizontal axis annotates the distance between the tip of the ablation catheter and the edge of the tissue. Negative distances correspond to positions inside the PV.

Fig. 8(b) adumbrates the edges of the tissue directly underneath the distal tip electrode. Higher current densities in the central line of scar compared to the surrounding tissue were caused by the higher conductivity of scar tissue.

D. Insertion Into a Pulmonary Vein

Fig. 9 shows characteristic LI traces for progressive introduction of an ablation catheter into the PV. Fig. 9(a) displays simulated LI values for the IntellaNav MiFi OI. The LI increased from 87 Ω in the simulated bloodpool up to peak values between 93 Ω and 176 Ω depending on the radius r_{PV} and the thickness th_{PV} of the PV. According LI traces for the IntellaNav Stablepoint are presented in Fig. 9(b). Starting from a simulated bloodpool LI of 139 Ω, the LI increased up to 145 Ω to 240 Ω depending on r_{PV} and th_{PV}.

The radius r_{PV} was found to be a strong determinant of the maximum LI reached upon insertion of the catheter into the PV. While the narrowest simulated PV with $r_{PV} = 2$ mm yielded a maximum LI of 176 Ω with the IntellaNav MiFi OI and 240 Ω with the IntellaNav Stablepoint, an increase of the radius by 1 mm resulted in a maximum LI of only 127 Ω and 186 Ω, respectively.

Peak values for all parameterizations of the PV corresponded with the insertion of the tip of the ablation catheter into the PV in the *in silico* experiments. The slight decrease for deeper insertions was related to the passing of the surrounding tissue plate that additionally elevated the LI at its maximum.

The thickness of the vein tissue took additional influence on the absolute LI value, as shown for a vein radius $r_{PV} = 6$ mm in Fig. 9.

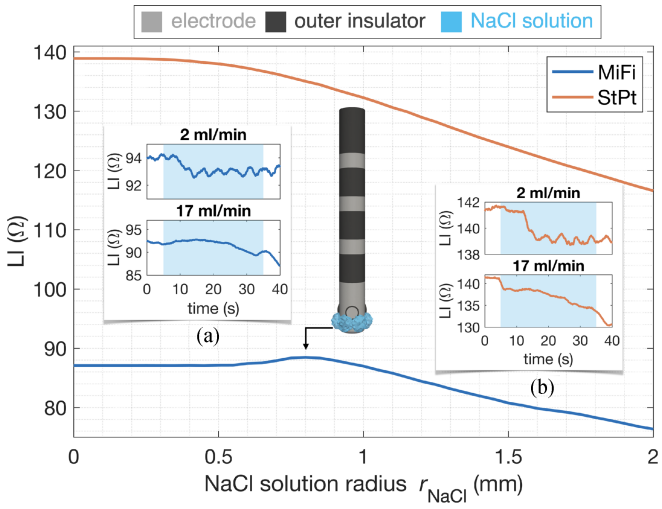

Fig. 10. *In silico* LI for different irrigation radii of NaCl solution for the IntellaNav MiFi OI in blue and the IntellaNav Stablepoint in orange. Subpanels (a) and (b) report *in vitro* measurements for the onset of irrigation flow rates of 2 $\frac{\text{ml}}{\text{min}}$ and 17 $\frac{\text{ml}}{\text{min}}$. Irrigation times are shaded in blue.

E. NaCl Solution Irrigation

Fig. 10 displays simulated LI values for flushing of the catheters with physiological NaCl solution exiting the cooling lumen at the irrigation holes. Varying the bubble radius r_{NaCl} from 0 to 2 mm mimicked changing the irrigation flow rate. The LI remained indifferent to NaCl bubbles up to a radius $r_{\text{NaCl}} = 0.7$ mm and $r_{\text{NaCl}} = 0.55$ mm with less than 1 % change compared to the *in silico* measurement in plain bloodpool of $87\,\Omega$ and $139\,\Omega$ for the IntellaNav MiFi OI and the the IntellaNav Stablepoint, respectively. For the IntellaNav MiFi OI, the LI then slightly increased reaching a maximum elevation of 1.4 Ω above the bloodpool for $r_{\text{NaCl}} = 0.8$ mm when the NaCl bubbles barely reached the mini electrodes' distal edges. Afterwards, LI values decreased with increasing r_{NaCl} down to 76.4 Ω for $r_{\text{NaCl}} = 2$ mm. The LI decreased monotonously for the IntellaNav Stablepoint down to 116.6 Ω for $r_{\text{NaCl}} = 2$ mm.

Fig. 10(a) and (b) display *in vitro* traces of LI for onset and offset of irrigation at different flow rates. *In vitro* measurements at a flow rate of 2 $\frac{\text{ml}}{\text{min}}$ revealed an instantaneous drop of 0.6 Ω and 1 Ω and oscillations in LI of 0.6 Ω and 1 Ω peak-to-peak amplitude tracing back to the cylinders of the irrigation wheel compressing the irrigation tube for the IntellaNav MiFi OI and the IntellaNav Stablepoint, respectively. For the IntellaNav Stablepoint, LI dropped abruptly by 2.5 Ω upon the onset of irrigation at 17 $\frac{\text{ml}}{\text{min}}$. The gradual decrease of LI is the result of a small bath volume mixing with the irrigation fluid of higher conductivity.

IV. Discussion

In summary, we presented an *in silico* environment that resembled *in human* and *in vitro* LI measurements to a high degree of detail and allowed for quantification of distinct influences on the measurement with known ground truth.

A. Aqueous NaCl Solutions

Model validation with standardized aqueous NaCl solutions of known conductivity was successful and proved the suitability of the simulation environment. NaCl solutions can be assumed to be of mostly resistive character at a measurement frequency of 14.5 kHz. Thus, the hyperbolic-like relationship between conductivity and LI can be explained as impedance reduces to resistance in this setup and resistance is reciprocally related to conductivity.

For *in vitro* experiments, aqueous NaCl solutions at 0.35 % to 0.4 % mass concentration at 21 °C were shown to serve well as dielectric equivalent of human blood at body temperature for a measurement frequency of 14.5 kHz.

A perfectly linear relationship between LI measurements with the IntellaNav MiFi OI and the IntellaNav Stablepoint as described by equation (1) is of great clinical value. Translation of findings and reference values between both catheters can extrapolate clinical trials to the respective other device and reduce efforts. Measurements with different instances of the catheters resulted in minor deviations of the linear coefficients and could potentially be caused by slight manufacturing differences or by the fact that all *in vitro* catheters had been used for radio frequency ablation before.

B. Transseptal Steerable Sheath

In silico experiments revealed that LI started to increase notably as soon as the sheath passed the proximal ring electrode. LI measurements for both, substrate and lesion characterization in clinical practice, should therefore always assure full withdrawal of the catheter out of the sheath in order to prevent confounding influences on the measured LI.

C. Catheter Tissue Interaction

The elevation of LI in tissue contact above the bloodpool LI ranged from $14\,\Omega$ for 0 mm distance to the tissue, i.e. 0 g so-called "contact force," to 33 Ω for -2 mm distance to the tissue and compared well to clinically observed mean ranges between $16\,\Omega$ and $20\,\Omega$ [27] for the IntellaNav MiFi OI. The simulated upper bound for an immersion depth of 2 mm thus likely overestimates the LI for clinical mean contact force applications due to the disregard of realistic tissue deformation.

Sulkin et al. had performed detailed *in vitro* experiments on catheter tissue interaction with the IntellaNav MiFi OI and found a nonlinear monotonic increase of LI as the catheter approximated the tissue at an angle of 90° [7]. The *in silico* results generated in this work matched the shape of the curve very well but yielded scaled absolute values and slopes presumably due to differences in the underlying conductivity of tissue and blood. The right ventricular tissue used by Sulkin et al. was presumably thicker than the atrial tissue modeled with a thickness of only 2.5 mm in this work and could explain the higher absolute values and slopes in their study. Additionally, the natural variability of the conductivity of tissue samples causes a spread of measured LIs [7] that could account for the scaled results. The specific conductivities chosen in this work are only one sample of the natural spread of human myocardial conductivity.

Changing the angle between catheter and tissue resulted in higher LIs for more parallel compared to orthogonal catheter orientation for distances $d_T > -2$ mm both in the work by Sulkin et al. and the *in silico* experiments in this work. Garrott et al. [8] observed a mean LI difference of 13 Ω between perpendicular and parallel catheter orientation of the IntellaNav StPt which is well in line with the *in silico* experiments presented here.

In silico experiments with the IntellaNav MiFi OI presented a small plateau for an immersion into atrial tissue by 1.0 mm to 1.5 mm as well as an abrupt decrease in LI for an angle $\alpha_T = 180\,^\circ$ that were not in line with the trend of the respective adjacent distances and angles. Presumably, the close interaction between the measuring mini electrode and the tissue caused both observations.

Clinical studies report different ranges of LI values for healthy and scar tissue, e.g. $109\,\Omega \pm 15\,\Omega$ and $104\,\Omega \pm 12\,\Omega$ [10], $111\,\Omega \pm 14\,\Omega$ and $92\,\Omega \pm 16\,\Omega$ [11], and $132\,\Omega \pm 12\,\Omega$ [12], respectively, for the IntellaNav MiFi OI. The variability in range may be explained by different operators and differences in typically applied contact force which remains uncontrolled for the IntellaNav MiFi OI. In line with previously published clinical observations, scar tissue presented lower LI compared to healthy myocardium due to the increase in extracellular space and the resulting increase in conductivity in the *in silico* model as well. Slightly lower values for both healthy and scar tissue in the *in silico* study as depicted in Fig. 7 in comparison with the clinical observations [10]–[12] could either be caused by the choice of conductivies in the *in silico* model or from a lower contact force. While the *in silico* model operates at an equivalent of 0 g so-called "contact force" for the experiments on scar tissue, typical clinical values range from 5 g to 20 g. The larger the lesion area within the footprint of the catheter, the lower the LI dropped. The results presented in Fig. 7 emphasize the importance of direct tissue contact and controlled contact force for quantitative applications of LI measurements. Drops in baseline LI caused by only 1 mm distance to the endocardial surface exceeded LI drops caused by transmural lesions. Since the exact values depend on the scar and tissue conductivity provided to the model and scar conductivity was approximated by the conductivity of connective tissue, a validation of the conductivity of atrial scar tissue would strengthen the finding but was out of the scope of this work.

Myocardial tissue was modeled as homogeneous, isotropic block. The effect of fiber direction and three-dimensional atrial structures remains unlit within the scope of this work. Future studies will have to shed light on more detailed models of the myocardium.

D. Insertion Into a Pulmonary Vein

In silico experiments demonstrated the strong dependency of the LI measured inside a PV on the radius of the vein. Vein tissue was modeled indifferently from myocardial tissue for simplicity although the substrates clearly differ histologically and can be assumed to further alter the LI measured in human PVs.

E. NaCl Solution Irrigation

Both IntellaNav MiFi OI and IntellaNav Stablepoint come with an open irrigated tip with the purpose of cooling the electrode during ablation delivery. Typically, catheters are flushed with 0.9 % so-called physiological NaCl solution at lab temperature. However, 0.9 % NaCl solution deviates by a factor of approximately 2 from human blood in terms of conductivity (compare Table I). Earlier studies have shown that the irrigation fluid during radio frequency ablation delivery takes influence on lesion formation. Highly conductive irrigation fluids such as physiological NaCl solution attract current flow and thus reduce the current flowing through the target tissue resulting in reduced energy deposition and smaller lesions compared to irrigation with less conductive fluids such as 0.45 % NaCl solution or dextrose water [28]–[31]. Similarly, awareness should be drawn to irrigation fluids for LI measurements during ablation delivery and substrate characterization. In particular, two cases have to be distinguished: the effect of constant irrigation flow rates $> 0\ \frac{\text{ml}}{\text{min}}$ and the effect of changing flow rates. Constant flow rates mainly relate to the application of LI substrate mapping while a change of flow rate alludes to the use case of radio frequency ablation delivery. In either case, clinical LI is mostly interpreted in differential manner comparing to the bloodpool reference or the LI at the start of the ablation as opposed to absolute values.

With the typical increase of the irrigation flow rate from a default flow of 2 $\frac{\text{ml}}{\text{min}}$ to 17 $\frac{\text{ml}}{\text{min}}$ or 30 $\frac{\text{ml}}{\text{min}}$ during radio frequency power delivery, the amount of irrigation fluid surrounding the catheter tip presumably increases and causes an LI drop by default that is not related to tissue heating as commonly attributed to LI drops during ablation. With the results presented in Fig. 10 and the assumption that the irrigation fluid is quickly flushed by circulatory blood flow, the LI drop caused by changes of the irrigation flow rate seem to be mostly negligible seen in the context of typically required minimum LI drops of 12 Ω to 16 Ω during radio frequency power delivery with the IntellaNav MiFi OI [9].

For the use case of LI substrate mapping, LI differences of few ohms become of importance. However, a constantly low flow rate of 2 $\frac{\text{ml}}{\text{min}}$ limits the potential for flawing the measurement. Interpreting LI only in differential manner, irrigation will impact the result if the distribution of NaCl close to the catheter tip changes, e.g. due to blood flow. Additionally, the higher conductivity of NaCl solution compared to tissue and blood causes less current to flow through the target of interest.

The *in silico* investigations in this work are clearly limited to the oversimplified spherical geometries of NaCl irrigation fluid at the catheter tip as well as the lack of a clear correlation between spherical radius in the model and clinical irrigation flow rates. Similarly, the *in vitro* setup lacks a model of circulatory blood flow. Including a fluid dynamics model could bring more detailed insights into the influence of irrigation and irrigation changes on the measured LI.

F. Sensitivity

Slight variations in the catheter dimensions resulted in notable changes of LI especially for the respective measuring electrodes.

For quantitative analyses, a detailed geometrical model of the catheter under investigation is therefore of high importance.

In silico experiments in this work demonstrated that selected phenomena of interest such as the presence of scar tissue result in minute changes in LI while recording conditions such as the loss of optimal wall contact cause changes in the same or even higher order of magnitude. In a clinical environment under the presence of measurement noise, the detectable range of changes in LI will further decrease, which emphasizes the necessity of establishing ideal wall contact, amongst other recording conditions under control of the operator.

In clinical setups, the inflation and deflation of the lungs is an additional confounding factor with evident impact on the LI measurement [27] due to the close proximity of the lungs to selected parts of the cardiac chambers. While the conductivity of inflated lungs is reported to be 0.0954 $\frac{\text{S}}{\text{m}}$ at 14.5 kHz, the conductivity increases to 0.247 $\frac{\text{S}}{\text{m}}$ in deflated state [21]. Since the respiratory state of the patient is a known parameter, respiratory oscillations in LI traces could be compensated for.

An estimate of the relative contribution of sample volumes in vicinity to the catheter to the measured LI would be of high interest in order to assess the suitability of catheters and electrode arrangements for impedance measurements. The close proximity of the catheter will take significantly more influence on the measured impedance for LI measurements as compared to generator impedance measurements. Specific examples such as varying the distance between catheter and tissue, scar, and sheath as well as varying the volume of NaCl irrigation fluid were presented in this work. However, a systematic analysis does not only require the variation of the sample volume position but also of its size and conductivity. Future studies should systematically shed light on this aspect in order to further optimize catheter and electrode arrangement for LI measurements.

V. Conclusion

With this work, we introduced and validated an *in silico* model including highly detailed catheter and sheath geometries in combination with a simplified myocardial geometry to study local electrical impedance measurements with intra-atrial catheters. Clinically relevant scenarios such as catheter-tissue interaction in terms of angle, distance, and substrate, the insertion of the catheter into a PV, the withdrawal into the transseptal sheath, and catheter irrigation were reflected in the model. Forward simulations of the electrical field gave insights in the quantitative effects of isolated and combined changes in parameters on the LI. The presented environment proved to be a highly valuable tool that provides deeper insight into the clinical interpretation of LI and has the potential to support future catheter development.

Acknowledgment

The authors would like to thank Tobias Oesterlein (Boston Scientific, Ratingen, Germany), Carina Jäger (Boston Scientific, Ratingen, Germany) and the always receptive EP nursing team at Städtisches Klinikum Karlsruhe for their support.

References

[1] S. Gabriel, R. W. Lau, and C. Gabriel, "The dielectric properties of biological tissues: II. Measurements in the frequency range 10 Hz to 20 GHz," *Phys. Med. Biol.*, vol. 41,, Apr. 1996, Art. no. 2251.

[2] S. Grimnes and O. G. Martinsen, *Bioimpedance and Bioelectricity Basics*, San London Diego: Academic Press, 2000.

[3] C. Reithmann et al., "Different patterns of the fall of impedance as the result of heating during ostial pulmonary vein ablation: Implications for power titration," *Pacing Clin. Electrophysiol.*, vol. 28, pp. 1282–1291, Jan. 2005.

[4] G. S. Chu et al., "Local impedance for the optimization of radiofrequency lesion delivery: A review of bench and clinical data," *J. Cardiovasc. Electrophysiol.*, vol. 33, pp. 389–400, Dec. 2021.

[5] P. C. Qian et al., "Optimizing impedance change measurement during radiofrequency ablation enables more accurate characterization of lesion formation," *JACC: Clin. Electrophysiol.*, vol. 7, pp. 471–481, Apr. 2021.

[6] R. van Es et al., "Novel method for electrode-tissue contact measurement with multi-electrode catheters," *EP Europace*, vol. 20, pp. 149–156, Jan. 2017.

[7] M. S. Sulkin et al., "Novel measure of local impedance predicts catheter-tissue contact and lesion formation," *Circulation. Arrhythmia Electrophysiol.*, vol. 11, Apr. 2018, Art. no. e005831.

[8] K. Garrott et al., "Combined local impedance and contact force for radiofrequency ablation assessment," *Heart Rhythm*, vol. 17, pp. 1371–1380, Aug. 2020.

[9] M. Das et al., "Local catheter impedance drop during pulmonary vein isolation predicts acute conduction block in patients with paroxysmal atrial fibrillation: Initial results of the LOCALIZE clinical trial," *EP Europace*, vol. 23, pp. 1042–1051, Feb. 2021.

[10] L. Segreti et al., "A novel local impedance algorithm to guide effective pulmonary vein isolation in atrial fibrillation patients: Preliminary experience across different ablation sites from the CHARISMA pilot study," *J. Cardiovasc. Electrophysiol.*, vol. 31, pp. 2319–2327, Jul. 2020.

[11] M. Gunawardene et al., "A novel assessment of local impedance during catheter ablation: Initial experience in humans comparing local and generator measurements," *EP Europace*, vol. 21, pp. i34–i42, Jan. 2019.

[12] C. A. Martin et al., "First clinical use of novel ablation catheter incorporating local impedance data," *J. Cardiovasc. Electrophysiol.*, vol. 29, pp. 1197–1206, Sep. 2018.

[13] P. Kauppinen, J. Hyttinen, and J. Malmivuo, "Sensitivity distribution visualizations of impedance tomography measurement strategies," *Int. J. Bioelectromagnetism*, vol. 8, pp. 63–71, Jan. 2006.

[14] INTELLANAV MIFI OPEN-IRRIGATED ABLATION CATHETER, Boston Scientific Corporation. 2018. Accessed: May 01, 2022. [Online]. Available: https://www.bostonscientific.com/content/dam/bostonscientific/Rhythm%20Management/general/EP-479201-AB_IntellaNav%20MiFi%20OI%20Spec%20Sheet%20FINAL.pdf

[15] INTELLANAV STABLEPOINT ABLATION CATHETER, Boston Scientific Corporation. 2020. Accessed: May 01, 2022. [Online]. Available: https://www.bostonscientific.com/content/dam/bostonscientific/ep/Electrophysiology%20Portfolio/Rhythmia/intellanav-stablepoint/EP-815001-AB_STABLEPOINT_SPECSHEET.pdf

[16] C. Geuzaine and J.-F. Remacle, "GMSH: A three-dimensional finite element mesh generator with built-in pre- and post-processing facilities," *Int. J. Numer. Methods Eng.*, vol. 79, no. 11, pp. 1309–1331, 2009.

[17] P. G. Platonov et al., "Left atrial posterior wall thickness in patients with and without atrial fibrillation: Data from 298 consecutive autopsies," *J. Cardiovasc. Electrophysiol.*, vol. 19, pp. 689–692, Feb. 2008.

[18] D. R. Lide and T. J. Bruno, *CRC Handbook of Chemistry and Physics*, vol. 99. Boca Raton, FL, USA: CRC Press, 2018.

[19] The effect of temperature on conductivity measurement; CONDUCTIVITY METER 4520 application note: A002-001 A. Accessed: Dec. 01, 2022. [Online]. Available: http://www.jenway.com/adminimages/A02_001A_Effect_of_temperature_on_conductivity.pdf

[20] H. Cao, M. A. Speidel, Jang-Zern Tsai, M. S. Van Lysel, V. R. Vorperian, and J. G. Webster, "FEM analysis of predicting electrode-myocardium contact from RF cardiac catheter ablation system impedance," *IEEE Trans. Biomed. Eng.*, vol. 49, no. 6, pp. 520–526, Jun. 2002.

[21] IT'IS Foundation, "Tissue properties database v4.0," May 2018.

[22] C. Gabriel, *Compilation of the Dielectric Properties of Body Tissues at RF and Microwave Frequencies*. Texas, USA: Occupational and Environmental Health Directorate, Radiofrequency Radiation Division, Brooks Air Force Base, Jan. 1996. Report N.AL/OE-TR-1996-0037.

[23] A. Adler and W. R. B. Lionheart, "Uses and abuses of EIDORS: An extensible software base for EIT," *Physiol. Meas.*, vol. 27, pp. S25–42, May 2006.

[24] K.-S. Cheng et al., "Electrode models for electric current computed tomography," *IEEE Trans. Biomed. Eng.*, vol. 36, no. 9, pp. 918–924, Sep. 1989.
[25] D. Bennett, "NaCl doping and the conductivity of agar phantoms," *Mater. Sci. Eng.: C*, vol. 31, pp. 494–498, Aug. 2011.
[26] M. A. Kandadai, J. L. Raymond, and G. J. Shaw, "Comparison of electrical conductivities of various brain phantom gels: Developing a 'brain gel model'," *Mater. Sci. Engineering: C*, vol. 32, pp. 2664–2667, Dec. 2012.
[27] L. A. Unger et al., "Local electrical impedance mapping of the atria: Conclusions on substrate properties and confounding factors," *Front. Physiol.*, vol. 12, Jan. 2022, Art. no. 788885.
[28] C. Gianni et al., "Half-normal saline versus normal saline for irrigation of open-irrigated radiofrequency catheters in atrial fibrillation ablation," *J. Cardiovasc. Electrophysiol.*, vol. 32, pp. 973–981, Jan. 2021.
[29] D. T. Nguyen et al., "Effect of irrigant characteristics on lesion formation after radiofrequency energy delivery using ablation catheters with actively cooled tips," *J. Cardiovasc. Electrophysiol.*, vol. 26, pp. 792–798, Jul. 2015.
[30] D. T. Nguyen et al., "Effect of environmental impedance surrounding a radiofrequency ablation catheter electrode on lesion characteristics," *J. Cardiovasc. Electrophysiol.*, vol. 28, pp. 564–569, Feb. 2017.
[31] D. T. Nguyen et al., "Radiofrequency ablation using an open irrigated electrode cooled with half-normal saline," *JACC: Clin. Electrophysiol.*, vol. 3, pp. 1103–1110, Oct. 2017.